Chapter 7
Nanoporous Anodic Alumina for Optical Biosensing

Abel Santos and Tushar Kumeria

Abstract As a result of its physical and chemical properties, nanoporous anodic alumina (NAA) has been envisaged as a promising nanomaterials for developing optical biosensing system with outstanding capabilities and performances. Recent studies have demonstrated that the combination of NAA with different optical techniques can yield a variety of innovative optical sensing systems for a broad range of analytes and applications. In this context, this chapter aims to report on the recent advances and developments of NAA-based optical biosensing systems. The different optical detection techniques, principles and concepts of NAA-based optical biosensing systems will be described in detail. Our objective is to provide a simple but detailed overview about the different NAA-based optical biosensing systems, with especial emphasis on the performance and capabilities of these devices. Finally, we will provide a future perspective on challenges and developments for this promising research field.

7.1 Introduction

Current technological advances have made it possible to implement sensing devices into technological gadgets present in our ordinary lives such as smart phones or computers [1–5]. This has generated new opportunities towards the development of easy-to-use sensing systems for a broad range of applications, ranging from detection of levels of glucose in blood to water quality analysis [1–4]. Regardless of these outstanding technological advances, extensive fundamental research is still needed in order to make this technology reliable, feasible, cost-competitive and

A. Santos (✉) · T. Kumeria
School of Chemical Engineering, The University of Adelaide,
North Engineering Building, Adelaide 5005, Australia
e-mail: abel.santos@adelaide.edu.au

D. Losic and A. Santos (eds.), *Nanoporous Alumina*,
Springer Series in Materials Science 219, DOI 10.1007/978-3-319-20334-8_7

efficient. Optical sensors are composed of three basic parts: namely; (i) the light source which generates optical waves, (ii) the sensing platforms where the interaction light-matter occurs and (iii) the detector where the shift in the optical signal is measured [6]. These three components will establish the sensing characteristics and performance of the optical sensor and thus are critical parameters to consider for developing optical sensing system with optimised capabilities. In particular, the sensing platform is a key element in any optical sensor given that it will establish the interaction light-matter and thus how different analytes are detected and quantified. Note that the interaction between light and matter produces changes in the characteristic optical signal of the sensing platform. Shifts in the characteristic optical signal are measured by the detector and a quantitative (concentration) and/or qualitative (spectral signature) relationship between analyte molecules and optical signal shifts can be established.

Different materials can be used to produce optical sensing platforms. These can be optically active or passive materials with capability to guide, reflect, absorb, transmit, emit, confine and/or enhance incident optical waves emitted by the source. In the last decade, the use of nanomaterials as optical sensing platforms has made it possible to develop optical sensing systems with outstanding capabilities and performances in terms of sensitivity, selectivity, versatility and applicability. Some examples of optical techniques that have been successfully combined with nanomaterials are surface-enhanced Raman spectroscopy (SERS), surface plasmon resonance spectroscopy (SPR), localised surface plasmon resonance spectroscopy (LSPR), reflectometric interference spectroscopy (RIFS) and photoluminescence (PL). Among the different materials used to develop optical sensing platforms, nanoporous anodic alumina (NAA) has been recently envisaged as a promising nanomaterial due to its unique set of physical and chemical properties [7, 8]. NAA is produced by the electrochemical anodisation of aluminium and its nanopores can be used as nanocontainers to accommodate, immobilise and detect a broad range of analytes in a selective manner (Fig. 7.1). The geometry of nanopores in NAA can be engineered through different electrochemical approaches, making it possible to design and engineer the effective medium of this nanoporous material in order to produce a variety of optical structures such as distributed Bragg refractors, waveguides, microcavities, omnidirectional mirrors, rugate filters and so on [7, 8]. Additionally, surface chemistry in NAA can be tuned according to specific sensing purposes by well-established chemistry protocols [9, 10].

This chapter is aimed at describing the most relevant optical biosensing systems based on NAA combined with different optical techniques. First, we will introduce different electrochemical approaches used to produce photonic structures based on NAA. After this, we will provide detailed descriptions of NAA-based optical biosensing systems, explaining their sensing principles, performances and practical applications. Finally, we will conclude this chapter with a prospective outlook on this field and its future challenges.

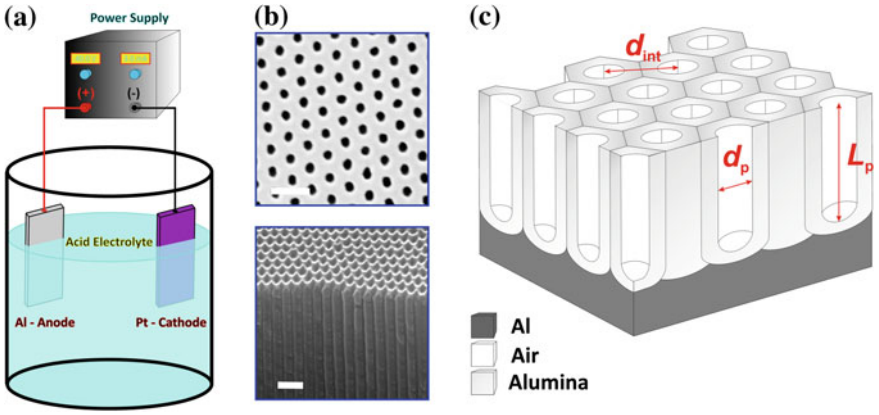

Fig. 7.1 Fabrication and geometric features of nanoporous anodic alumina. **a** Schematic illustration describing a basic electrochemical anodisation cell used to produce NAA. **b** Top and cross-section scanning electron microscopy (SEM) images of NAA (scale bars = 400 and 250 nm, respectively). **c** Scheme describing the most representative geometric features of NAA (i.e. d_p pore diameter, L_p pore length and d_{int} interpore distance)

7.2 Structural Engineering of Nanoporous Anodic Alumina

Electrochemical anodisation of high purity aluminium foils under specific conditions yields nanoporous anodic alumina structures. This nanofabrication technique, which was originally used in industrial processes such as metal surface finishing, machinery and automobile engineering, corrosion protection and so forth, was adopted by nanotechnology in the 1950s after electronic microscopes revealed the nanoporous nature of the aluminium oxide layers produced by anodisation of aluminium [11]. In particular, Keller characterised the structure of NAA for the first time by electron microscopy. This study revealed that NAA is composed of hexagonally arranged arrays of nanopores, in which the distance between adjacent nanopores (i.e. interpore distance) is directly proportional to the anodisation voltage [12]. This work was followed by a flood of studies aimed to characterise the physical and chemical properties of NAA structures produced under different conditions. Furthermore, pioneering theoretical models explaining the formation mechanism of NAA were proposed by Diggle in 1968 [13]. In the next years, Thompson and Wood made good use of new characterisation techniques such as microtome sectioning and transmission electron microscopy in order to understand the different phenomena playing a role in the formation mechanism of NAA [14, 15]. These studies established the anion and water incorporation mechanisms in the structure of NAA, which take place in the course of the anodisation process. After this, numerous theoretical models about the pore nucleation and growth mechanism in NAA were postulated [16–24]. However, the actual mechanism of NAA growth

has yet to be completely clarified. In general, it is assumed that pore nucleation starts in the oxide thin film formed on the aluminium surface at the early stages of the anodisation process. Defects and pits located on the surface of that oxide layer along with instabilities in the electric field across it generate electric field concentrations at certain sites on the surface of the oxide film. These sites become nucleating centres for nanopore formation, where the electric field becomes focused, the ionic conduction enhanced and the local temperature increased by Joule effect. In this way, the oxide layer is preferentially dissolved at these sites and nanopores start to grow through the surface of the oxide film. After nucleation, nanopores grow until a steady state of growth is achieved. At this point, the flux of ionic species across the oxide barrier layer is in equilibrium and nanopores grow at constant rate (Fig. 7.2).

The flood of studies and intensive research carried out during these decades originated the seminal works of Masuda and co-workers, which are considered as the most important milestones in the use of NAA in nanotechnology [25–28]. Masuda and co-workers introduced the two-step anodisation process and reported on the self-organisation conditions in the most commonly used acid electrolytes

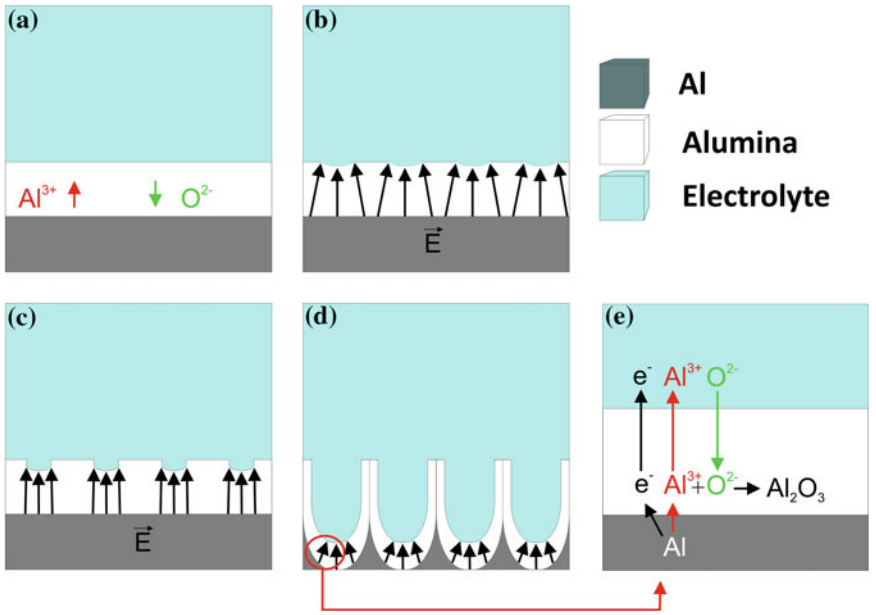

Fig. 7.2 Schematic cross-section diagram describing the first stages of growth of NAA. **a** Formation of a thin, compact layer of Al_2O_3. **b** Instabilities in the electric field across the oxide film dissolve partially the oxide at certain sites (i.e. nucleating centres). **c** Pore formation at the nucleating centres on the aluminium oxide surface. **d** Steady growth of pores (i.e. competition between formation and dissolution of aluminium oxide). **e** Magnified view of the *red circle* in (**d**) showing the transport of the main ionic species through the oxide barrier layer at the pore *bottom tips*

(i.e. sulphuric (H_2SO_4), oxalic ($H_2C_2O_4$) and phosphoric acids (H_3PO_4)). In this electrochemical approach, after the first anodisation step, the resulting NAA layer is chemically dissolved. The result is a pattern of hexagonally arranged hemispherical nanoconcavities on the surface of the aluminium substrate. These nanoconcavities enable the self-organised growth and propagation from top to bottom of cylindrical nanopores in the course of the second anodisation step, which is conducted under the same conditions as the first anodisation step. This simple but cost-effective and elegant anodisation approach makes it possible to produce highly organised NAA structures without the use of lithographic methods or expensive laboratory facilities. Self-organised NAA can be described as a nanoporous matrix of aluminium oxide (Al_2O_3—alumina) that features close-packed arrays of hexagonal cells containing a cylindrical nanopore at the centre. Nanopores grow perpendicularly to the underlying aluminium substrate. NAA is typically produced in electrolytes composed of aqueous solutions of acids, in which the anode (i.e. aluminium foil) and cathode (e.g. platinum) are immersed. The anodisation process starts when certain anodisation voltage or current is applied between anode and cathode. Then, nanopores nucleate and start to grow perpendicularly to the aluminium substrate. The growth of nanopores in steady state is a result of a competing electrochemical process between oxidation (i.e. formation of oxide) and dissolution (i.e. oxide dissolution) through the oxide barrier layer at the nanopore bottom tips. In this process, aluminium oxide grows at the interface aluminium-alumina as a result of the countermigration of ionic species through the oxide barrier layer. At the same time, alumina is dissolved at the interface alumina-electrolyte. Electrochemical anodisation of aluminium can be basically described by the following reduction-oxidation equations:

(i) Formation of alumina—aluminium-alumina interface (anode)

$$2Al(s) + 3H_2O(l) \rightarrow Al_2O_3(s) + 6H^+(aq) + 6e^- \tag{7.1}$$

(ii) Dissolution of alumina—alumina-electrolyte interface (anode)

$$Al_2O_3(s) + 6H^+(aq) \rightarrow 2Al^{3+}(aq) + 3H_2O(l) \tag{7.2}$$

(iii) Diffusion of aluminium cations—within oxide barrier layer (anode)

$$2Al(s) \rightarrow 2Al^{3+}(aq) + 6e^- \tag{7.3}$$

(iv) Hydrogen evolution—electrolyte-cathode interface (cathode)

$$6H^+(aq) + 6e^- \rightarrow 3H_2(g) \tag{7.4}$$

Note that, apart from the above electrochemical reaction, side reactions such as oxygen evolution at the anode take place in the course of the anodisation process. Therefore, the experimental current efficiency is always lower than 100 % during the

electrochemical anodisation of aluminium. Aluminium can be anodised to produce NAA under two different regimes, so-called mild anodisation (MA) and hard anodisation (HA) [11, 25–28]. MA is conducted at moderate voltages and temperatures, while HA is carried out at high voltages and low temperatures. It is worth stressing that MA and HA conditions are dependent on the acid electrolyte. Another characteristic feature of these anodisation regimes is the growth rate, which is constant and slow under MA conditions (i.e. 3–8 μm h^{-1}) and exponentially decreasing and extremely fast at HA regime (i.e. 50–70 μm h^{-1}). As far as the geometric features of the resulting NAA structures, these can be defined by the pore diameter (d_p), pore length (L_p) and interpore distance (d_{int}). These geometric features can be precisely engineered by the anodisation conditions within the range of 10–400 nm for d_p, from a few nanometres to hundreds of micrometres for L_p and 50–600 nm for d_{int} [29, 30]. Table 7.1 compiles the geometric features of NAA structures produced under the most commonly used MA and HA anodisation conditions.

In terms of chemical composition, the structure of NAA presents an onion-like chemical distribution with an outer layer composed of aluminium oxide contaminated with impurities from the electrolyte and an inner layer basically composed of pure alumina [28] (Fig. 7.3). However, some studies have revealed that the actual chemical structure of NAA is divided into more than two chemical layers [31, 32]. In a study reported by Yamamoto et al., the chemical structure of NAA was analysed by studying its photoluminescence spectrum [31]. The obtained results revealed that the chemical structure of NAA is divided into three layers, with decreasing content of impurities from the central pore to the outer pore walls. Recently, Santos et al. analysed the chemical composition of NAA by studying its chemical dissolution in real-time by reflectometric interference spectroscopy [32]. These results revealed that the actual chemical structure of NAA is composed of up to four stratified chemical layers with increasing concentration of impurities from the inner side of the pores (i.e. layer close to the cell walls) to the outer side of the pores (i.e. layer close to the pore walls).

Note that the optical properties of NAA are directly related to its chemical composition and nanoporous structure. The structure of nanopores in NAA can be engineered by different electrochemical approaches in order to produce a variety of optical nanostructures with precisely designed optical properties. In this way, the

Table 7.1 Summary of the most widespread fabrication conditions used to produce NAA by mild (MA) and hard anodisation (HA) of high purity aluminium substrates along with the geometric features of the resulting nanostructures

Acid electrolyte	Anodisation regime	V (V)	T (°C)	d_p (nm)	d_{int} (nm)	Growth rate (μm h^{-1})	References
$H_2C_2O_4$ 0.3 M	HA	140	0–1	50	280	50	[11]
$H_2C_2O_4$ 0.3 M	MA	40	5–8	30	100	3.5	[25]
H_2SO_4 0.3 M	MA	25	5–8	25	63	7.5	[26]
H_3PO_4 0.1 M	MA	195	0–1	160	500	2	[27]
H_2SO_4 0.3 M	HA	40	0–1	30	78	85	[51]

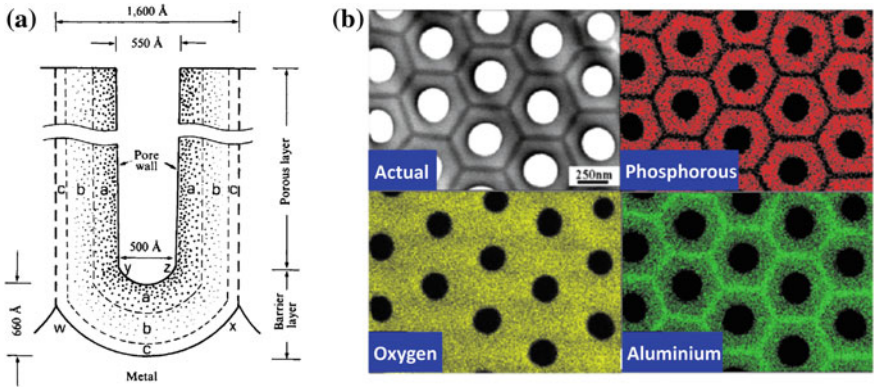

Fig. 7.3 Chemical structure of NAA. **a** Cross-section diagram showing the distribution of chemical impurities in the structure of NAA (adapted from [31]). **b** X-ray maps of elements distributed in the structure of NAA (adapted from [30])

Table 7.2 Compilation of the most representative pore geometries in NAA produced by different electrochemical approaches

Type of NAA	Electrochemical approach	References
Funnel-like	Combination of multiple anodisation and pore widening steps	[33–38]
Multilayered	Stepwise or pulse anodisation	[39–43]
Serrated	Anodisation at low voltage and high temperature	[44, 45]
Hierarchical	Asymmetric two-step anodisation	[46, 47]
Three-dimensional	Modulated anodisation profile and final wet chemical etching	[48, 49]
Modulated	Modulated anodisation profile	[50–52]

interaction between light and matter can be engineered in order to guide, confine, transmit, emit or reflect light in a selective manner for different purposes and applications. So far, optical nanostructures based on NAA have demonstrated a promising potential to be used as sensing platforms for developing optical biosensing systems. In that respect, it is worthwhile noting the versatility of NAA in terms of pore architecture, which can present nanopores with funnel-like [33–38], multilayered [39–43], serrated [44, 45], hierarchical [46, 47], three-dimensional [48, 49] and modulated [50–52]. Table 7.2 compiles some of the most common examples of NAA architectures produced by different electrochemical approaches.

Among these, the generation of pore diameter modulations in the course of the anodisation process has been intensively researched in the last years. Different electrochemical approaches have made it possible to modulate the pore diameter of NAA in depth and produce a variety of pore shapes with precisely controlled geometric features. Figure 7.4 summarises the most representative strategies used to modulate the pore diameter of NAA. Pore diameter modulations in NAA were

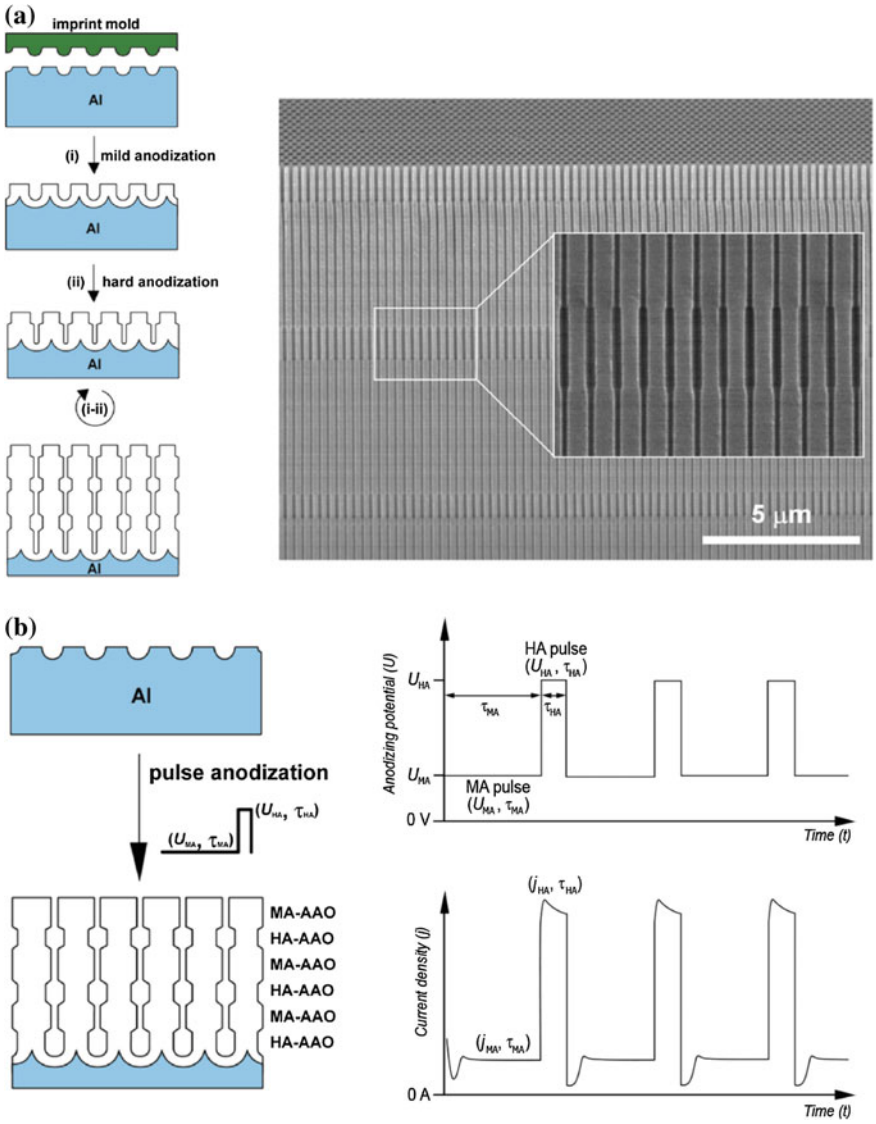

Fig. 7.4 Generation of pore diameter modulations in NAA. **a** Discontinuous nanopore modulation (adapted from [30]). **b** Continuous nanopore diameter by pulse anodisation (adapted from [30])

pioneered by Lee et al. by switching the anodisation conditions between MA to HA regimes [11]. To this end, the surface of electropolished aluminium substrates was patterned by a master stamp with hexagonally arranged arrays of nanopyramids prior to anodisation. The period of these nanopyramids (i.e. distance between the centre of adjacent nanopyramids) was 275 nm and the anodisation conditions of the first step were set to match that interpore distance under MA regime (i.e. H_3PO_4

0.4 M at 110 V and 10 °C for 15 min). As a result of that patterning stage nanopores grew in an organised arrangement from top to bottom in a single anodisation step. Then, the anodisation conditions were modified from MA to HA using an aqueous solution of oxalic acid 0.015 M at 137 V and 0.5 °C for 2 min. By repeating this process in a sequential cyclic fashion, they were able to modulate the diameter of nanopores in NAA from top to bottom. In this approach Lee et al. made good use of the different porosity levels between MA (10 %) and HA (3 %) conditions in oxalic acid as well as the fact that the interpore distance was the same under these conditions, preventing nanopores from branching after the anodisation conditions were changed. Furthermore, the length of each segment (i.e. MA or HA segments) was precisely controlled by the anodisation time, enabling the generation of NAA structures with exquisitely engineered geometric features from top to bottom. Although this work was the starting point of a flood of studies, this electrochemical approach has some inherent limitations given that a pre-patterning stage must be used and the acid electrolyte has to be changed after every anodisation step. In that respect, pulse anodisation, which is an electrochemical approaches based on voltage or current density pulses, made it possible to overcome these limitations and thus modulate the pore diameter in NAA in a simply manner [39, 50–52]. Among the different properties of NAA featuring pore diameter modulations, its optical properties are particularly interesting as they can be used to develop a variety of optical nanostructures for sensing applications.

Multilayered NAA is another type of structures with interesting optical properties, which can be used to develop sensing systems. These optical nanostructures are generated by changing the level of porosity between stacks of layers of NAA by switching the anodisation profile in the course of the anodisation process [39–43]. Note that different anodisation profiles such as saw-like, stepwise, sinusoidal or pseudosinusoidal can be used to design the effective medium of NAA by structural engineering. These electrochemical approaches have been used to produce NAA-based optical platforms such as microcavities, rugate filters, distributed Bragg reflectors, waveguides and omnidirectional mirrors. Lee et al. used a pulse anodisation approach under potentiostatic conditions in order to create multilayers of NAA in sulphuric acid electrolyte [39]. In this study, periodic stepwise voltage pulses between MA and HA regimes were used to design the nanoporous architecture of NAA along the pore length by introducing pore diameter modulations (Fig. 7.5). Making a good use of this approach, Sulka et al. demonstrated a NAA-based distributed Bragg reflector (DBR) structure [40]. In this approach, NAA was first produced by pulse anodisation in order to engineer its effective refractive index in depth. Then, the surface area of NAA was selectively infiltrated with polymer by using transmission electron microscopy grids as masks. The resulting NAA-based DBR mirrors showed enhanced reflection of light at two different ranges of wavelength. Zheng et al. produced NAA-based DBR structures by a pseudosinusoidal anodisation profile under voltage control [41]. This study demonstrated that the characteristic transmission peak of these DBR structures can be tuned within the visible spectrum by changing the temperature of the electrolyte. Furthermore, Santos et al. analysed the pore rearrangement phenomenon during the

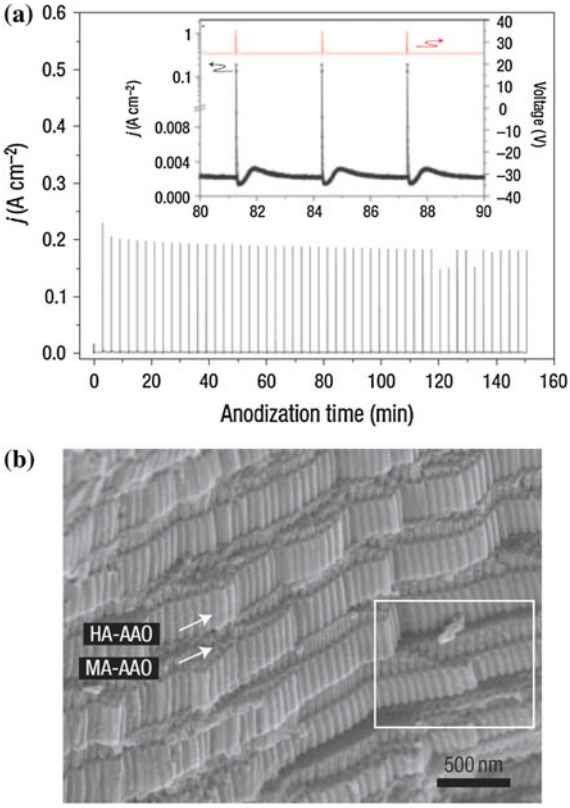

Fig. 7.5 Generation of multilayered nanostructures based on NAA by pulse anodisation. **a** Anodisation profile (adapted from [39]). **b** Cross-section SEM image of the resulting multilayered NAA structure (adapted from [39])

MA to HA regime transition studying the formation of bilayered NAA structures [42]. In this study, different parameters such as the anodisation voltage ramp and the HA voltage were systematically analysed in order to obtain a better understanding of the arrangement of nanopores when the anodisation regime is changed. These nanostructures can be used to develop bilayered NAA optical structures such as complex Fabry–Pérot interferometers. In a more recent work, Rahman et al. fabricated NAA-based DBR structures by a cyclic anodisation approach under voltage control [53]. In this study, a direct relationship between the photonic stop-band of the resulting NAA structures and the pore diameter was established, demonstrating that the photonic stop-band of these DBR structures can be engineered by modifying the pore diameter of NAA.

Funnel-like NAA is another type of structure with interesting optical properties, which can be used to develop optical biosensing systems [33–38]. Typically, this type of nanostructure is fabricated by combining sequential anodisation and pore widening steps in a discontinuous fashion (Fig. 7.6). The resulting NAA structures are composed of a stack of layers of NAA featuring decreasing pore diameter from top to bottom, which can range from a bilayered to a multilayered structure, depending on the number of anodisation and pore widening steps. As far as the

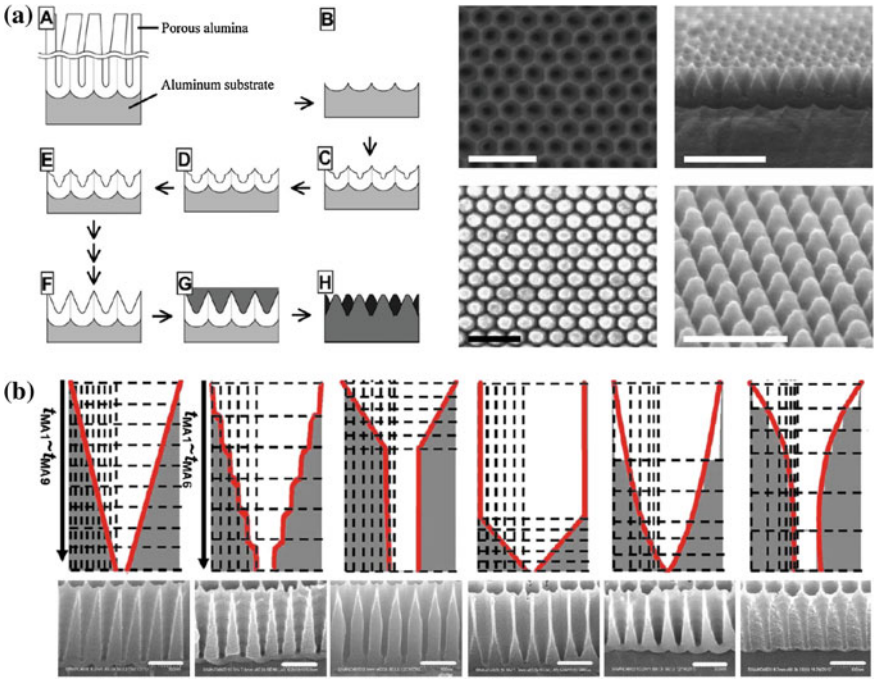

Fig. 7.6 Generation of funnel-like nanostructures based on NAA sequential combination of multiple anodisation and pore widening steps. **a** Fabrication process for low aspect ratio *funnel-like* NAA and SEM images of templates and nickel replicas (adapted from [35]). **b** Anodisation profiles and cross-section SEM image of *funnel-like* NAA structures featuring different geometries and shapes (adapted from [38])

fabrication process is concerned, this starts with an anodisation step, which is followed by a pore widening step. This process is repeated in a sequential fashion in order to engineer the nanoporous structure of NAA in depth. Note that funnel-like NAA structures can be used as templates to produce other nanostructures based on different materials such as polymers or metals by replica synthesis. The resulting nanostructures have interesting optical properties for different purposes such as antireflection coatings or optical biosensors. In that regard, He et al. replicated the inner structure of funnel-like NAA in order to produce shape-coded silica nanotubes, which were used as optical biosensing platforms for multiplexed immunoassays [33]. Another study by Nagaura et al. reported on the fabrication of funnel-like NAA featuring low aspect ratio (i.e. multi-short segments of NAA featuring smoothly decreased pore diameter from top to bottom) [34]. This work was extended by the same authors, who used these templates in order to create nickel-based replicas [35]. The resulting metallic films featured nanocones distributed across the surface according to the pattern established by the funnel-like NAA template. In another study, Yanagishita et al. made good use of funnel-like NAA structures in order to developed antireflection coatings based on polymers

[36]. These films were created by photoimprinting approach using funnel-like NAA templates featuring different pore geometry. After fabrication, the resulting polymer-based films were optically evaluated by studying their transmittance spectra. The obtained results revealed that smoother changes in the inner structure of the funnel-like NAA structure provide lower reflectance. Another study by Santos et al. reported on the fabrication of high aspect ratio funnel-like NAA structures (i.e. multi-long segments of NAA featuring smoothly decreased pore diameter from top to bottom) [37]. In this work, the length of each segment in the funnel-like structure was controlled by the total charge (i.e. total current charge passed through the system during each anodisation step), enabling a precise control over the length of each segment. In a more recent study, Li et al. tailored the inner shape of funnel-like NAA structures by combining anodisation and pore widening steps of different lengths [38]. They were able to generate whorl-embedded cones, funnels, pencils, linear cones, trumpets and parabolas in the inner nanoporous structure of NAA by this electrochemical approach. Traditionally, funnel-like NAA structures are produced featuring cylindrical nanopores with decreasing pore diameter from top to bottom. Nevertheless, Santos et al. reported on a unique electrochemical approach aimed to generate inverted funnel-like structures [32]. This type of NAA structure was produced by a sequential combination of anodisation and annealing steps with a final pore widening step. The resulting funnel-like structures feature increasing pore diameter from top to bottom. Note that, taking advantage of the optical properties of NAA, the formation process of inverted funnel-like structures was monitored in real-time by reflectometric interference spectroscopy, making it possible to precisely engineer their structure.

7.3 Optical Biosensors Based on NAA Structures

As mentioned above, nanostructures based on NAA have a unique set of optical properties that can be used to develop optical biosensing systems. As a result of its outstanding electronic and optical properties, porous silicon has been intensively researched in the last decades to produce a variety of optical sensing platforms. However, regardless of these properties, porous silicon has some inherent limitations such as disorganised nanoporous structure, fragility and poor chemical stability under harsh conditions. In that respect, NAA offers multiple advantages such as chemical stability under acidic or basic conditions, mechanical robustness, well-defined nanoporous structure and functional surface chemistry [54–56]. These assets make NAA a promising candidate for developing optical sensing systems and an alternative nanomaterial to traditional porous silicon sensing platforms. Recently, an extensive research work has been devoted to developing NAA-based optical sensing systems. Here, we will report on the most outstanding advances in the design, development and applicability of these optical sensing systems. Table 7.3 summarises the most representative examples of these optical systems and their sensing capabilities.

Table 7.3 Summary of optical biosensors based on NAA platforms

Sensing system	Analyte	Detection limit	References
SERS-NAA	p-Aminothiophenol	0.5 M	[58]
	4-Mercaptopyridine	$1 \cdot 10^{-6}$ M	[59]
	3-Mercaptobenzoic	3 mM	[61]
	Benzenethiol	500 ppb	[62]
	N-Methyl-4-nitroaniline	3 ppb	[62]
SPR-NAA	Avidin	10 μg mL^{-1}	[69]
	Anti-5-fluorouracil	100 mg mL^{-1}	[69]
	Melittin	100 ng mL^{-1}	[69]
	$Ru[BPhen_3]^{2+}$	2 μM	[64]
	$Fe[Phen_3]^{2+}$	1 μM	[64]
	BSA	60 nM	[65]
	Invertase	10 nM	[35]
RIfS-NAA	H_2S	0.5 v%	[83]
	DNA	2 nmol cm^{-2}	[81]
	Circulating tumour cells	1000 cells mL^{-1}	[82]
	Immunoglobulin	0.1 mg mL^{-1}	[79]
	Glucose	100 mM	[85]
	Cysteine	5 mM	[85]
	Gold(III)	0.1 μM	[86]
	BSA	1 mg mL^{-1}	[87]
	Glucose	0.01 M	[88]
	BSA	15 μM	[82]
	Human IgG	600 nM	[84]
PL-NAA	Morin	$5 \cdot 10^{-6}$ M	[97]
	Trypsin	40 μg mL^{-1}	[97, 100]
		0.1 mg mL^{-1}	
	DNA	100 mM	[98]
	Oxazine 170	$6.5 \cdot 10^{-3}$ M	[99]
	Glucose	0.1 M	[99]
	Glucose	10 mM	[85]
	Cysteine	5 mM	[85]

Detection technique, analyte and detection limit

7.3.1 *Surface-Enhanced Raman Scattering (SERS)*

Surface-enhanced Raman scattering spectroscopy (SERS) is an ultra-sensitive optical technique based on the enhancement of Raman scattering that takes place when biomolecules are absorbed on the surface of metal films featuring nano-structured roughness. This optical phenomenon has been associated with the excitation of localised surface plasmons on the surface of metallic nanostructures,

which are known as “hot spots” or “hot junctions”. However, a complete explanation of the actual mechanism involved in SERS is still to come. In the last decade, many studies have made good use of SERS as a powerful analytical technique in order to detect a broad range of analytes with implications in many research fields. Raman signals from biomolecules adsorbed onto the surface of SERS substrates can be enhanced around six orders of magnitude as compared to other analytical techniques, making it possible to achieve limits of detection as low as single molecules. Furthermore, SERS is not only a quantitative technique but also qualitative as biomolecules present characteristic SERS signals, which can be used as fingerprints for identification (i.e. spectroscopy signature). Among the different nanomaterials used to develop SERS substrates, NAA has showed a very promising potential as a result of its well-organised nanometric structure, which can be precisely replicated to produce metallic substrates with nanometric features, and its scalable and cost-efficient fabrication process.

NAA-based SERS substrates can be fabricated by depositing metals such as gold or silver on the top or bottom surface of NAA templates by thermal evaporation or sputtering. Nonetheless, other approaches have been used to produce NAA-based SERS substrates. Some examples of these are metallic membranes, decoration of nanopores with nanoparticles and growth of nanowires (Fig. 7.7). As mentioned before, the geometric features of NAA structures can be precisely engineered by the anodisation conditions, which along with the metal deposition conditions enable the fabrication of SERS substrates with optimised optical signals for specific sensing

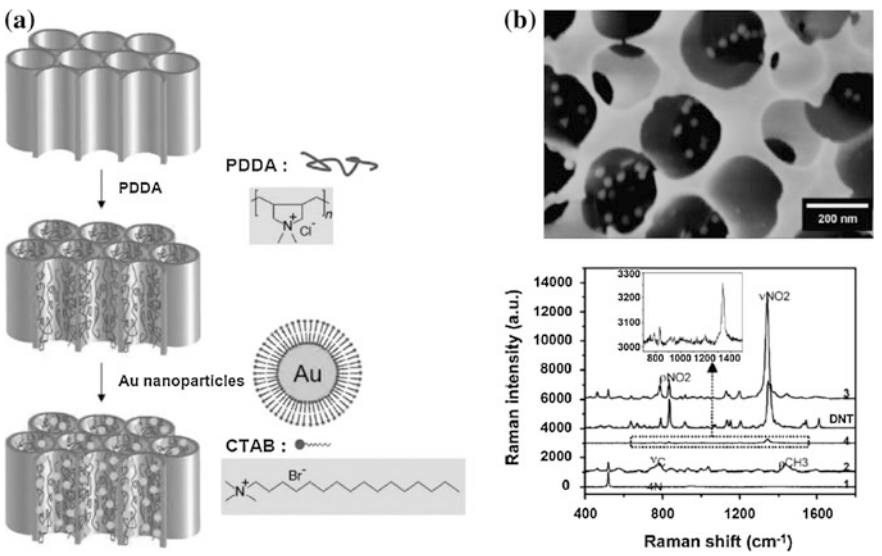

Fig. 7.7 NAA-based SERS systems. **a** Fabrication process for a NAA-based SERS substrate based on gold nanoparticles (adapted from [57]). **b** SEM image of the resulting SERS system and its sensing performance (adapted from [57])

purposes. For example, the inner surface of nanopores in NAA substrates was decorated with gold nanoparticles by Ko et al. [57]. The resulting NAA-based SERS substrates were used to detect trace amounts of an aromatic compound of TNT-based plastic explosive (i.e. 2,4-dinitrotoluene), which cannot be detected by conventional Raman spectroscopy. A similar approach was used by Lu et al., who decorated the inner surface of nanopores in NAA substrates with silver nanoparticles [58]. In this approach, silver nanoparticles were grown by incubation in an electrolyte composed of $Ag(NH_3)^{2+}$, which was subsequently reduced to silver nanoparticles.

Then, SERS signals were optimised as a function of the size and density of silver nanoparticles when detecting p-aminothiophenol. Note that a point-by-point SERS mapping of analyte molecules immobilised onto these NAA-based SERS substrates was used to characterise the homogeneity of adsorbed molecules across these substrates. In another approach, Ji et al. developed NAA-based SERS substrates by electrodepositing silver nanoparticles on the inner surface of NAA substrates [59]. The homogeneity and stability of the resulting SERS substrates were optimised by studying the effect of different electrodeposition times. The sensing performance of these NAA-based SERS substrates was evaluated by detecting 4-mercaptopyridine molecules. Using a different approach, Lee et al. developed NAA-based SERS substrates by electrodepositing silver nanowires inside NAA templates [60]. The sensing performance of the resulting optical sensing platforms was optimised by analysing the effect of the distance between adjacent nanowires within the alumina matrix when detecting 4-aminobenzenethiol. Their results revealed that the intensity of SERS signals can be enhanced up to 200-fold by reducing the intergap distance from 35 to 10 nm. Valleman et al. made good use of an electroless deposition approach inside NAA membranes [61]. The resulting gold-NAA composite membranes were used as SERS substrates to characterise the formation of monolayers of 3-mercaptobenzoic acid. It was reported that the resulting gold structure featured a slight curvature along the nanopores, which increased the SERS effect from the middle to the bottom of the nanopores. Recently, the inner surface of NAA substrates was decorated with silver nanocubes by Kodiyath et al., who used a layer-by-layer deposition approach based on polyelectrolytes [62]. The sensing performance of these NAA-based SERS substrates was evaluated by detecting trace levels of organic vapours of benzenethiol and N-methyl-4-nitroaniline. The obtained results demonstrated that these nanostructures can provide efficient, reliable and versatile sensing capabilities and that the limit of detention and saturation level are directly related to the number of polyelectrolyte bilayers deposited onto the inner surface of NAA nanopores. Furthermore, it was reported a direct and strong relationship between the density and distribution of silver nanocubes and the sensing performance. Finally, this study compared the sensing performance of silver nanocubes and nanoparticles, demonstrating that the former metallic nanostructures can provide better sensing capabilities and performances for the above-mentioned vapour analytes (Fig. 7.8).

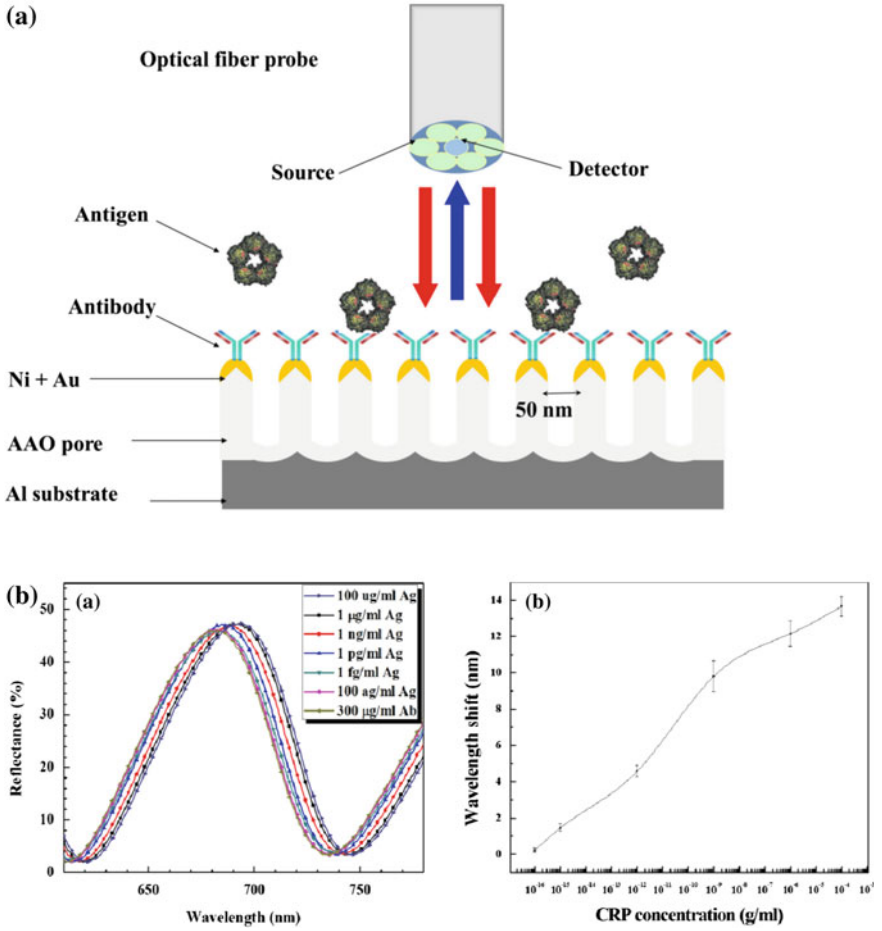

Fig. 7.8 NAA-based LSPR systems. **a** Structure of a LSPR system based on NAA coated with *gold* and chemically functionalised with antibodies to target C-reactive protein antigens (adapted from [70]). **b** Sensing performance of that system when detecting C-reactive protein (adapted from [70])

7.3.2 Surface Plasmon Resonance (SPR)

Similarly to SERS, surface plasmon resonance (SPR) is based on the generation of surface plasmons from an evanescent electromagnetic wave. This phenomenon occurs when a light beam is focused on the surface of a prism coated with a thin metallic film. This optical technique is typically implemented in a Kretschmann configuration. NAA structures can be used to develop unique SPR sensing systems. The most widespread method to produce NAA-based SPR systems is to grow a layer of NAA on the surface of a thin aluminium film deposited on the surface of

the prism [63]. In this system, the plasmonic properties depend on the effective medium of the adjacent nanoporous matrix within distances of several hundreds of nanometres. For this reason, any change in the effective medium inside the nanopores of the NAA film is translated into a shift in the SPR signal, making it possible to quantify and detect trace levels of analyte molecules. Furthermore, NAA-based SPR systems can be used to monitor in real-time and in situ biological events taking place inside the nanopores such as adsorption or desorption of molecules, association or dissociation of specific interactions between ligands or digestion of proteins. It is worthwhile mentioning that NAA-based SPR systems can be designed to provide improved sensing performances by engineering the nanoporous structure of the NAA film. In this way, light can be guided and confined in a selective manner, minimising losses associated with scattering effects [64]. Lau et al. and Koutsioubas et al. developed NAA-based SPR systems capable of monitoring the adsorption and desorption of bovine serum albumin (BSA) molecules inside the nanopores of NAA films in real-time and establishing the effect of pH on these processes [65, 66]. In another study, Dhathathreyan used a NAA-based SPR system in order to determine the kinetics of digestion of sucrose by enzyme invertase [67]. First, enzyme molecules were immobilised onto the inner surface of NAA nanopores and the digestion of sucrose to produce glucose and fructose was characterised in real-time as a function of pH by SPR. The obtained results demonstrated that this digestion process presents a biphasic kinetic for both the absorption of enzyme molecules and the digestion of sucrose. Lau et al. reported on the use of a NAA-based SPR system to characterise the grafting of poly (g-benzyl-L-glutamate) inside the nanopores, taking as a reference the surface of planar silicon dioxide substrates [68]. The obtained results confirmed that the conformation of the polymeric nanostructure inside the nanopores of NAA was a result of polymer chains confinement. Hotta et al. demonstrated that the sensing performance of NAA-based SPR systems can be significantly improved by engineering the structure of the NAA film [64]. To this end, they optimised the sensing performance of this system as a function of the pore geometry when detecting the adsorption of BSA molecules. They reported an enhanced red shift of more than 300 nm as compared to other NAA-based SPR system without optimised nanoporous structure.

It is worth stressing that SPR systems based on NAA structures are not only limited to a Kretschmann configuration. Localised surface plasmon resonance (LSPR) systems based on NAA platforms have been intensively researched as well. These systems are composed of highly ordered arrays of metallic nanoparticles such as gold or silver, which are deposited on the top or bottom surfaces of NAA substrates. The resulting metallic nanostructures feature organised arrangement at nanometric scale and can provide unique sensing performances for a broad range of analytes and applications. Hiep et al. developed a NAA-based LSPR system by depositing gold nanoparticles on the top surface of NAA substrates [69]. The sensing capabilities of that system were evaluated by detecting specific interactions between biotin/avidin and 5-fluorouracil/anti-5-fluorouracil. The obtained results demonstrated that this system provides a significant enhancement in terms of

detection as a result of combined SPR and interference effects. Making good use of this, Yeom et al. fabricated an immunosensor to detect C-reactive protein [70]. In this system, gold nanoparticles were first deposited on the surface of NAA substrates and C-reactive protein antibodies immobilised onto theses LSPR platforms. Subsequently, C-reactive protein antigen molecules were selectively detected, achieving a low limit of detection as low as 1 fg mL^{-1}. Kim et al. developed a similar LSPR system, which was used to detect picomolar concentrations of untagged oligonucleotides when they hybridise with synthetic and PCR-amplified DNA molecules [71].

7.3.3 *Reflectometric Interference Spectroscopy (RIfS)*

Another highly sensitive and intensively researched optical technique is reflectometric interference spectroscopy (RIfS), which relies on the interaction between a white light beam and a thin film [72]. Gauglitz pioneered the use of RIfS for biosensing applications by combining RIfS with sensing platforms composed of polymer films based on polyethylene glycols and dextrans [73]. Typically, thin films of these polymers are applied onto different substrates such as silicon dioxide or glass and, subsequently, recognition elements for biomolecules such as antibodies, aptamers, esterone and phospholipid membranes are immobilized onto them. The resulting molecular interaction causes a quantifiable change in the effective optical thickness of the film, which results in a modulation of the interference spectrum. Therefore, to monitor this change over time makes it possible to characterise the binding behaviour of target molecules. Another important contribution to the development of biosensing systems based on RIfS was made by Sailor, who combined porous silicon platforms with RIfS in order to develop a variety of highly sophisticated sensing systems for a broad range of applications [74, 75]. Porous silicon-based RIfS systems have emerged as an outstanding alternative to traditional polymer thin films [76, 77]. Recently, some studies have reported on the development of NAA-based RIfS systems, which have showed a very promising potential. These systems could become an complementary alternative to porous silicon systems, providing some superior advantages in terms of chemical and mechanical stability, controllable pore geometry, scalable and cost-competitive fabrication process [7, 8] (Fig. 7.9). The RIfS spectrum of NAA structures presents a well-resolved interference pattern produced by the Fabry–Pérot effect, which is defined by $2n_{eff}L_p = m\lambda$, where n_{eff} is the effective refractive index of NAA, L_p is the physical thickness of the NAA film, and m is the order of the RIfS fringe, the maximum of which is located at the wavelength λ [78]. Note that RIfS is a label-free technique and thus makes it possible to follow biological events in real-time and in situ without the use of fluorescence or radioactive labels. NAA-based RIfS systems are able to perform ultra-sensitive detection of analytes such as organic gases and biomolecules in a quantitative and qualitative manner [79, 80]. Pan et al. developed a NAA-based RIfS system for label-free detection of

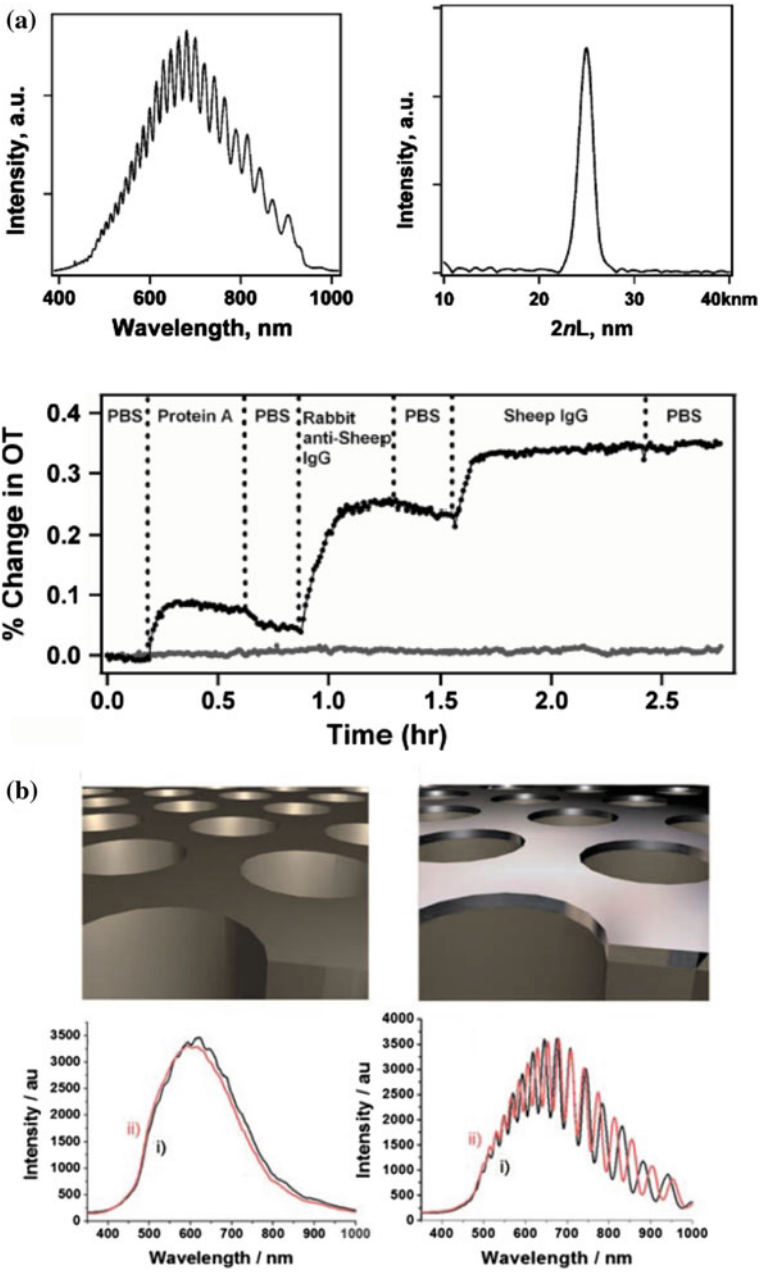

Fig. 7.9 NAA-based RIfS systems. **a** Sensing principle of a NAA-RIfS system and real-time monitoring of antibody-antigen interactions (adapted from [79]). **b** Enhancement of RIfS signals in NAA by coating its *top surface* with thin films of metal (adapted from [84])

complementary DNA molecules [81]. In another interesting study, Alvarez et al. fabricated a label-free immunosensor based on the combination of RIfS with NAA platforms [79]. This system was capable of selectively monitor binding interactions between antibodies and antigens, confirming that these produce a significative change in the effective optical thickness when the interaction is specific. Kumeria et al. made good use of this characteristic in order to develop a microchip biosensor based on RIfS and NAA platforms to detect and quantify circulating tumour cells (CTCs) [82]. NAA substrates were first coated with a thin layer of gold, which was subsequently functionalised with biotinylated anti-EpCAM antibodies aimed at capturing and detecting CTCs in a single step. Furthermore, these authors used a similar system to detect volatile sulphur and hydrogen sulphide compounds associated with malodour [83]. First, NAA platforms were coated with thin films of metals and monolayers of functional molecules were immobilised onto them in order to endow these sensors with chemical selectivity towards target gas molecules. Another NAA-based RIfS system was developed by Dronov et al., who fabricated an interferometric transducer by coating NAA platforms with platinum [84]. This study demonstrated that thin metal films on the top surface of NAA platforms enhance the interferometric pattern in RIfS, increasing the signal-to-noise ratio by LSPR effect. Furthermore, this study compared the sensing performance of these platforms with traditional porous silicon. The obtained results revealed that NAA is more sensitive than porous silicon, providing more stable and reliable optical signals. Note that the sensing performance of the proposed system was evaluated by detecting two types of immunoglobulin antibodies, anti-BSA and anti-human IgG. In another study, Santos et al. compared the sensing performance of NAA-based RIfS and photoluminescence sensors based on the same nanoporous sensing platform (vide infra) [85]. These sensors were assessed when detecting different analytes under non-specific and specific adsorption conditions. To this end, optical signals were optimised as a function of the pore geometry in both spectroscopic techniques. Then, the most optimal sensing platform was established by comparing the sensing performance when detecting D-glucose and L-cysteine under non-specific and specific adsorption conditions, respectively. These results showed that the nature of the analyte molecule and the adsorption conditions are key parameters in the resulting sensing performance of these optical systems. In addition, these results revealed that NAA platforms combined with photoluminescence present a better sensing performance than that of NAA-based RIfS platforms, with a better linearity, higher sensitivity and lower limit of detection. Recently, Kumeria et al. developed a NAA-based RIfS system capable of performing ultra-sensitive detection of gold ions in aqueous solutions [86]. First, NAA substrates were chemically functionalised with 3-mercaptopropyl-tirethoxysilane (MPTES) in order to endow these sensing platforms with chemical selectivity towards gold ions. The sensing principle in this system relies on the effective optical thickness change that takes place when gold ions are immobilised by thiol groups present of the inner surface of NAA nanopores. The sensing performance of this system was assessed by establishing the linear range, saturation concentration, sensitivity and low limit of detection. Furthermore, these authors demonstrated the

applicability of this system for real-life scenarios through a series of experiments using different media such as buffer solution and tap water. In another study, Macías et al. made good use of a bilayered funnel-like NAA structure to develop a NAA-based RIfS system [87]. The RIfS spectrum of these sensing platforms presented a complex series of Fabry–Pérot interference fringes, which were studied when detecting BSA molecules. NAA-based rugate filters were developed by Kumeria et al. in order to demonstrate the direct relationship between sensing performance and the nanoporous structure of NAA [88]. This system, the sensing principle of which was based on shifts in the characteristic peak position of the rugate filter structure, was assessed when detecting different levels of glucose in a non-specific manner. Small changes in the effective medium of the nanoporous material produced shifts in the characteristic peak position, making it possible to discern the most sensitive NAA structure as a function of the nanoporous structure. Finally, the obtained results were verified with the Looyenga–Landau–Lifshitz model. An extension of this work was reported by the same authors, who demonstrated these NAA-based DBR structures are capable of performing detection of low concentrations of mercury ions in tap and river water [89].

In addition to the above mentioned sensing capabilities, NAA-based RIfS systems can be used to monitor the release of molecules from these nanoporous substrates. Making good use of this property, Kumeria et al. were able to study the release of indomethacin, an anti-inflammatory drug, from NAA substrates under dynamic flow conditions through changes in the effective optical thickness of the nanoporous platform [90]. This study demonstrated that this process is controlled by the diffusion of drug molecules from the nanopores to the eluting medium and that this is directly related with the flow rate. These results revealed that the faster the flow rate the faster the release of drug molecules from the nanoporous substrate. In contrast to traditional static conditions, this system provides more reliable information that can help to engineer drug-releasing implants with improved capabilities for in vivo applications.

7.3.4 Photoluminescence Spectroscopy (PLS)

Nanoporous anodic alumina is a well-known photoluminescent material, the properties of which have been intensively studied during the last decades. However, the actual origin of its photoluminescent properties is still a matter of debate [91–93]. It is generally accepted that PL in NAA relies on two types of photoluminescent centres. F-centres are associated with the total amount of impurities incorporated into the chemical structure of NAA from the acid electrolyte in the course of the anodisation process [94]. F^+-centres are related to ionised oxygen vacancies present in the amorphous structure of NAA [92, 93]. Therefore, the PL properties of NAA are highly dependent on the fabrication conditions such as the acid electrolyte, the anodisation voltage/current density, the anodisation regime and thermal treatments [91, 95, 96]. As far as the use of these PL properties for sensing

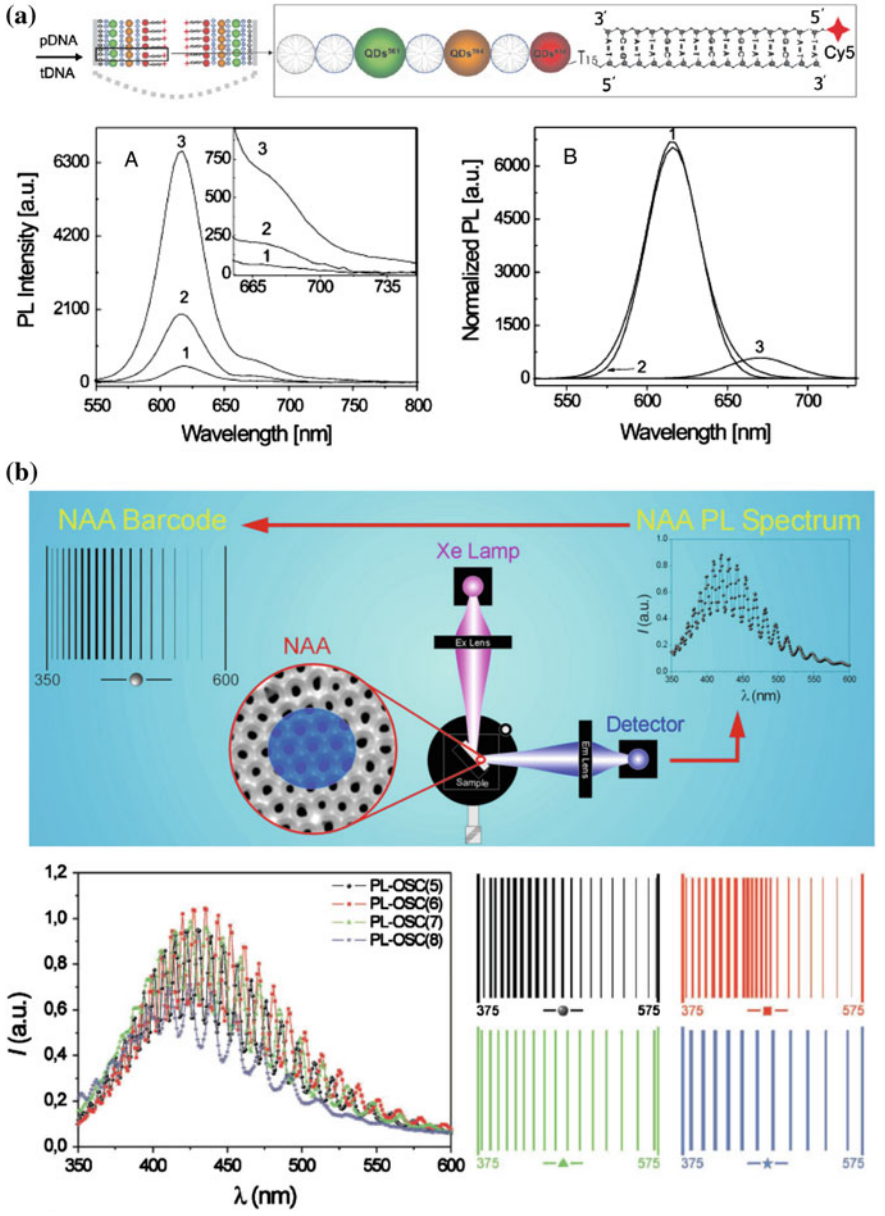

Fig. 7.10 NAA-based PLS systems. **a** PL-NAA biosensing platform developed to monitor DNA hybridisation through changes in the PL spectrum of NAA (adapted from [98]). **b** Optical barcode system based on PL-NAA biosensing platforms (adapted from [99])

purposes, pioneering studies used NAA substrates to accommodate, immobilise and detect analyte molecules through changes in the PL spectrum of NAA platforms. Ji et al. detected non-fluorescent morin and morin-trypsin infiltrated in the nanoporous network of NAA substrates using as a sensing principle shifts in the PL spectrum of these platforms [97]. The obtained results revealed chemical interactions between morin molecules and alumina. Feng et al. developed a more sophisticated system capable of monitoring the hybridisation of DNA molecules immobilised onto the nanoporous structure of NAA [98]. In this system, the inner surface of NAA nanopores was chemically functionalised with mercaptoundecanoic acid. This was followed by layer-by-layer deposition of positively and negatively charged dendrimers, intercalating layers of ZnCdSe quantum dots.

This NAA-based PL system demonstrated enhanced sensitivity afforded by the use of photoluminescent quantum dots, which enable the detection of the hybridisation of DNA molecules (Fig. 7.10a). Furthermore, a direct relationship between the assemblies of quantum dots and the sensitivity of the system was established. Santos et al. pioneered a barcode system for sensing applications based on the PL spectrum of NAA substrates in the UV-visible region [99]. Likewise in RIfS, the PL spectrum of NAA presents well-resolved and narrow oscillations as a result of interferometric effect, which amplifies and enhances the emission of light from the NAA structure (Fig. 7.10b). These oscillations correspond to the optical modes of the optical cavity formed by the NAA film and can be used to develop optical sensors as any change in the effective medium is translated into shifts in these characteristic oscillations. This principle was used to develop a barcode system for sensing applications, which was demonstrated by detecting organic molecules such as organic dyes, enzymes and glucose [99, 100].

7.4 Conclusions

As this chapter has shown, NAA has become the nanomaterial of choice to develop a variety of nanostructures with outstanding physical and chemical properties. Particularly interesting are the optical properties of these nanostructures as nanopores in NAA can be engineered through different electrochemical approaches in order to reflect, guide, emit, transmit and confine light in a selective manner and create a variety of optical sensing platforms with unique capabilities and performances. Here, we have summarised the most representative fundamental aspects related with the structural engineering of NAA aimed at producing optical nanostructures. Furthermore, we have presented in detail some outstanding combinations of optical sensing techniques NAA photonic structures such as SERS, SPR, LSPR, RIfS and PLS. These studies have demonstrated that the key features of NAA such as scalable and cost-efficient fabrication process, versatile nanopore geometry, chemical and mechanical stability and optical properties make this nanomaterial a promising alternative to conventional sensing platforms.

There are still excellent opportunities for further developments of optical biosensing systems based on NAA structures. Particularly interesting are the implementation of these systems into lab-on-a-chip devices with separation, detection and quantification capabilities for multiple analytes. Furthermore, the development of implantable biosensors for in vivo applications and the development of point-of-care systems for medical and environmental diagnosis are thought to be two areas of focus for future applications of NAA-based optical sensors.

Acknowledgments Financial support from Australian Research Council (DE14010054) and the School of Chemical Engineering of The University of Adelaide are greatly acknowledged.

References

1. Q. Wei, R. Nagi, K. Sadeghi, S. Feng, E. Yan, S.J. Ki, R. Caire, D. Tseng, A. Ozcan, Detection and spatial mapping of mercury contamination in water samples using a smart-phone. ACS Nano **2**, 1121–1129 (2014)
2. Q. Wei, H. Qi, W. Luo, D. Tseng, S.J. Ki, Z. Wan, Z. Göröcs, L.A. Bentolila, T.T. Wu, R. Sun, A. Ozcan, Fluorescent imaging of single nanoparticles and viruses on a smart phone. ACS Nano **10**, 9147–9155 (2013)
3. S. Khatua, M. Orrit, Toward single-molecule microscopy on a smart phone. ACS Nano **10**, 8340–8343 (2013)
4. S. Ayas, A. Cupallari, O.O. Ekiz, Y. Kaya, A. Dana, Counting molecules with a mobile phone camera using plasmonic enhancement. ACS Photonics **1**, 17–26 (2014)
5. Y.D. Ivanov, T.O. Pleshakova, N.V. Krohin, A.L. Kaysheva, S.A. Usanov, A.I. Archakov, Registration of the protein with compact disk. Biosens. Bioelectron. **43**, 384–390 (2013)
6. J. Homola, S.S. Yee, G. Gauglitz, Surface plasmon resonance sensors: review. Sens. Actuators, B **54**, 3–15 (1999)
7. A. Santos, T. Kumeria, D. Losic, Nanoporous anodic alumina: a versatile platform for optical biosensors. Materials **7**, 4297–4320 (2014)
8. T. Kumeria, A. Santos, D. Losic, Nanoporous anodic alumina platforms: engineered surface chemistry and structure for optical sensing applications. Sensors **14**, 11878–11918 (2014)
9. F. Rusmini, Z. Zhong, J. Feijen, Protein immobilization strategies for protein biochips. Biomacromolecules **8**, 1775–1789 (2007)
10. C.J. Ingham, J. ter Maat, W.M. de Vos, Where bio meets nano: the many used of nanoporous aluminium oxide in biotechnology. Biotechnol. Adv. **30**, 1089–1099 (2012)
11. W. Lee, R. Ji, U. Gösele, K. Nielsch, Fast fabrication of long-range ordered porous alumina membranes by hard anodization. Nat. Mater. **5**, 741–747 (2006)
12. F. Keller, M.S. Hunter, D.L. Robinson, Structural features of oxide coatings on aluminum. J. Electrochem. Soc. **100**, 411–419 (1953)
13. J.W. Diggle, T.C. Downie, C.W. Coulding, Anodic oxide films on aluminum. Chem. Rev. **69**, 365–405 (1969)
14. J.P. O'Sullivan, G.C. Wood, The morphology and mechanism of formation of porous anodic films on aluminium. Proc. R. Soc. London, Ser. A **317**, 511–543 (1970)
15. G.E. Thompson, G.C. Wood, Anodic films on aluminum. *Treatise on materials science and technology*, vol. 23 (Academic Press, New York, 1983)
16. T.P. Hoar, N.F. Mott, A mechanism for the formation of porous anodic oxide films on aluminium. J. Phys. Chem. Solids **9**, 97–99 (1959)
17. V.P. Parkhutik, V.I. Shershulsky, Theoretical modelling of porous oxide growth on aluminum. J. Phys. D Appl. Phys. **25**, 1258–1263 (1992)

18. G. Patermarakis, P. Lenas, C.H. Karavassilis, G. Papayiannis, Kinetics of growth of porous anodic Al_2O_3 films on Al metal. Electrochim. Acta **36**, 709–725 (1991)
19. G. Patermarakis, N. Papandreadis, Study on the kinetics of growth of porous anodic Al_2O_3 films on Al metal. Electrochim. Acta **38**, 2351–2361 (1993)
20. G. Patermarakis, D. Tzouvelekis, Development of a strict kinetic model for the growth of porous anodic Al_2O_3 films on aluminium. Electrochim. Acta **39**, 2419–2429 (1994)
21. G. Patermarakis, H.S. Karayannis, The mechanism of growth of porous anodic Al_2O_3 films on aluminium at high film thicknesses. Electrochim. Acta **40**, 2647–2656 (1995)
22. G. Patermarakis, Transformation of the overall strict kinetic model governing the growth of porous anodic Al_2O_3 films on aluminium to a form applicable to the non-stirred bath film growth. Electrochim. Acta **41**, 2601–2611 (1996)
23. J. Randon, P.P. Mardilovich, A.N. Govyadinov, R. Paterson, Computer-simulation of inorganic membrane morphology Part 3 anodic alumina films and membranes. J. Colloid Interface Sci. **169**, 335–341 (1995)
24. S.K. Thamida, H.C. Chang, Nanoscale pore formation dynamics during aluminum anodization. Chaos **12**, 240–251 (2002)
25. H. Masuda, K. Fukuda, Ordered metal nanohole arrays made by a two-step replication of honeycomb structures of anodic alumina. Science **268**, 1466–1468 (1995)
26. H. Masuda, F. Hasegwa, Self-ordering of cell arrangement of anodic porous alumina formed in sulfuric acid solution. J. Electrochem. Soc. **144**, L127–L130 (1997)
27. H. Masuda, K. Yada, A. Osaka, Self-ordering of cell configuration of anodic porous alumina with large-size pores in phosphoric acid solution. Jpn. J. Appl. Phys. **37**, L1340–L1342 (1998)
28. K. Nielsch, J. Choi, K. Schwirn, R.B. Wehrspohn, U. Gösele, Self-ordering regimes of porous alumina: the 10 % porosity rule. Nano Lett. **2**, 677–680 (2002)
29. G.D. Sulka, Highly ordered anodic porous alumina formation by self-organized anodizing, in *Nanostructured Materials in Electrochemistry*, vol. 1, ed. by A. Eftekahari (Wiley-VCH Verlag GmbH and Co. KGaA, Weinhem, Germany, 2008), pp. 1–116
30. W. Lee, S.J. Park, Porous anodic aluminium oxide: anodization and template synthesis of functional nanostructures. Chem. Rev. **114**, 7487–7556 (2014)
31. Y. Yamamoto, N. Baba, S. Tajima, Coloured materials and photoluminescence centres in anodic film on aluminium. Nature **289**, 572–574 (1981)
32. A. Santos, T. Kumeria, Y. Wang, D. Losic, *In situ* monitored engineering of inverted nanoporous anodic alumina funnels: on the precise generation of 3D optical nanostructures. Nanoscale **6**, 9991–9999 (2014)
33. B. He, S.J. Son, S.B. Lee, Suspension array with shape-coded silica nanotubes for multiplexed immuno assays. Anal. Chem. **79**, 5257–5263 (2007)
34. T. Nagaura, F. Takeuchi, S. Inoue, Fabrication and structural control of anodic alumina films with inverted cone porous structure using multi-step anodizing. Electrochim. Acta **53**, 2109–2114 (2008)
35. T. Nagaura, F. Takeuchi, Y. Yamauchi, K. Wada, S. Inoue, Fabrication of ordered Ni nanocones using porous anodic alumina template. Electrochem. Commun. **10**, 681–685 (2008)
36. T. Yanagishita, T. Kondo, K. Nishio, H. Masuda, Optimization of antireflection structures of polymer based on nanoimprinting using anodic porous alumina. J. Vac. Sci. Technol., B **26**, 1856–1859 (2008)
37. A. Santos, P. Formentín, J. Pallarès, J. Ferré-Borrull, L.F. Marsal, Structural engineering of nanoporous anodic alumina funnels with high aspect ratio. J. Electroanal. Chem. **655**, 73–78 (2011)
38. J. Li, C. Li, C. Chen, Q. Hao, Z. Wang, J. Zhu, X. Gao, Facile method for modulating the profiles and periods of self-ordered three-dimensional alumina taper-nanopores. ACS Appl. Mater. Interfaces **4**, 5678–5683 (2012)

39. W. Lee, K. Schwirn, M. Steinhart, E. Pippel, R. Scholz, U. Gösele, Structural engineering of nanoporous anodic aluminium oxide by pulse anodization of aluminium. Nat. Nanotechnol. **3**, 234–239 (2008)
40. G.D. Sulka, K. Hnida, Distributed Bragg reflector base on porous anodic alumina fabricated by pulse anodization. Nanotechnology **23**, 075303 (2012)
41. W.J. Zheng, G.T. Fei, B. Wang, L.D. Zhang, Modulation of transmission spectra of anodized alumina membrane distributed Bragg reflector by controlling anodization temperature. Nanoscale Res. Lett. **4**, 665–667 (2009)
42. A. Santos, J.M. Montero-Moreno, J. Bachmann, K. Nielsch, P. Formentín, J. Ferré-Borrull, J. Pallarès, L.F. Marsal, Understanding pore rearrangement during mild to hard transition in bilayered porous anodic alumina membranes. ACS Appl. Mater. Interfaces **3**, 1925–1932 (2011)
43. M.M. Rahman, L.F. Marsal, J. Pallarès, J. Ferré-Borrull, Tuning the photonic stop bands of nanoporous anodic alumina-based distributed Bragg reflectors by pore widening. ACS Appl. Mater. Interfaces **5**, 13375–13381 (2013)
44. D. Li, L. Zhao, C. Jiang, J.G. Lu, Formation of anodic aluminum oxide with serrated nanochannels. Nano Lett. **10**, 2766–2771 (2010)
45. X. Zhu, L. Liu, Y. Song, H. Jia, H. Yu, X. Xiao, X. Yang, Oxygen bubble mould effect: serrated nanopore formation and porous alumina growth. Monatshefte Chem. **139**, 999–1003 (2008)
46. J.M. Montero-Moreno, M. Sarret, C. Müller, Some considerations on the influence of voltage in potentiostatic two-step anodizing of AA1050. J. Electrochem. Soc. **154**, C169–C174 (2007)
47. A. Santos, J. Ferré-Borrull, J. Pallarès, L.F. Marsal, Hierarchical nanoporous anodic alumina templates by asymmetric two-step anodization. Phys. Status Solidi A **208**, 668–674 (2011)
48. D. Losic, D. Losic Jr, Preparation of porous anodic alumina with periodically perforated pores. Langmuir **25**, 5426–5431 (2009)
49. A. Santos, L. Vojkuvka, M. Alba, V.S. Balderrama, J. Ferré-Borrull, J. Pallarès, L.F. Marsal, Understanding and morphology control of pore modulations in nanoporous anodic alumina by discontinuous anodization. Phys. Status Solidi A **209**, 2045–2048 (2012)
50. K. Pitzschel, J.M. Montero-Moreno, J. Escrig, O. Albrecht, K. Nielsch, J. Bachmann, Controlled introduction of diameter modulations in arrayed magnetic iron oxide nanotubes. ACS Nano **3**, 3463–3468 (2009)
51. K. Schwirn, W. Lee, R. Hillebrand, M. Steinhart, K. Nielsch, U. Gösele, Self-ordered anodic aluminum oxide formed by H_2SO_4 hard anodization. ACS Nano **2**, 302–310 (2008)
52. D. Losic, M. Lillo, D. Losic Jr, Porous alumina with shaped pore geometries and complex pore architectures fabricated by cyclic anodization. Small **5**, 1392–1397 (2009)
53. M.M. Rahman, E. García-Caurel, A. Santos, L.F. Marsal, J. Pallarès, J. Ferré-Borrull, Effect of the anodization voltage on the pore-widening rate of nanoporous anodic alumina. Nanoscale Res. Lett. **7**, 474 (2012)
54. A. Santos, T. Kumeria, D. Losic, Nanoporous anodic aluminum oxide for chemical sensing and biosensors. Trends Anal. Chem. **44**, 25–38 (2013)
55. M. Stephan, I. Mey, C. Steinem, A. Janshoff, Combining reflectometry and fluorescence microscopy: an assay for the investigation of leakage processes across lipid membranes. Anal. Chem. **86**, 1366–1371 (2014)
56. H. Neubacher, I. Mey, C. Carnarius, T.D. Lazzara, C. Steinem, Permeabilization assay for antimicrobial peptides based on pore-spanning lipid membranes on nanoporous alumina. Langmuir **30**, 4767–4774 (2014)
57. H. Ko, V.V. Tsukruk, Nanoparticle-decorated nanocanals for surface-enhanced Raman scattering. Small **4**, 1980–1984 (2008)
58. Z. Lu, W. Ruan, J. Yang, W. Xu, C. Zhao, B. Zhao, Deposition of Ag nanoparticle on porous anodic alumina for surface enhanced Raman scattering substrate. J. Raman Spectrosc. **40**, 112–116 (2009)

59. N. Ji, W. Ruan, C. Wang, Z. Lu, B. Zhao, Fabrication of silver decorated anodic aluminum oxide substrate and its optical properties on surface-enhanced Raman scattering and thin film interference. Langmuir **25**, 11869–11873 (2009)
60. S.J. Lee, Z. Guan, H. Xu, M. Moskovits, Surface-enhanced Raman spectroscopy and nanogeometry: the plasmonic origin of SERS. J. Phys. Chem. C **111**, 17985–17988 (2007)
61. L. Velleman, J.L. Bruneel, F. Guillaume, D. Losic, J.G. Shapter, Raman spectroscopy probing of self-assembled monolayers inside the pores of gold nanotube membranes. Phys. Chem. Chem. Phys. **13**, 19587–19593 (2011)
62. R. Kodiyath, S.T. Malak, Z.A. Combs, T. Koenig, M.A. Mahmoud, M.A. El-Sayed, V.V. Tsukruk, Assemblies of silver nanocubes for highly sensitive SERS chemical vapor detection. J. Mater. Chem. A **1**, 2777–2788 (2013)
63. R.J. Green, R.A. Frazier, K.M. Shakesheff, M.C. Davies, C.J. Roberts, S.J.B. Tendler, Surface plasmon resonance analysis of dynamic biological interactions with biomaterials. Biomaterials **21**, 1823–1835 (2000)
64. K. Hotta, A. Yamaguchi, N. Teramae, Nanoporous waveguide sensor with optimized nanoarchitectures for highly sensitive label-free biosensing. ACS Nano **6**, 1541–1547 (2012)
65. K.H.A. Lau, L.S. Tan, K. Tamada, M.S. Sander, W. Knoll, Highly sensitive detection of processes occurring inside nanoporous anodic alumina templates: a waveguide optical study. J. Phys. Chem. B **108**, 10812–10818 (2004)
66. A.G. Koutsioubas, N. Spiliopoulos, D. Anastassopoulos, A.A. Vradis, G.D. Priftis, Nanoporous alumina enhanced surface plasmon resonance sensors. J. Appl. Phys. **103**, 094521 (2008)
67. A. Dhathathreyan, Real-time monitoring of invertase activity immobilized in nanoporous aluminium oxide. J. Phys. Chem. B **115**, 6678–6682 (2011)
68. K.H.A. Lau, H. Duran, W. Knoll, *In situ* characterization of N-carboxy anhydride polymerization in nanoporous anodic alumina. J. Phys. Chem. B **113**, 3179–3189 (2009)
69. H.M. Hiep, H. Yoshikawa, E. Tamiya, Interference localized surface plasmon resonance nanosensor tailored for the detection of specific biomolecular interactions. Anal. Chem. **82**, 1221–1227 (2010)
70. S.H. Yeom, O.G. Kim, B.H. Kang, K.J. Kim, H. Yuan, D.H. Kwon, H.R. Kim, S.W. Kang, Highly sensitive nano-porous lattice biosensor based on localized surface plasmon resonance and interference. Opt. Express **19**, 22882–22890 (2011)
71. D.K. Kim, K. Kerman, M. Saito, R.R. Sathuluri, T. Endo, S. Yamamura, Y.S. Kwon, E. Tamiya, Label-free DNA biosensor based on localized surface plasmon resonance coupled with interferometry. Anal. Chem. **79**, 1855–1864 (2007)
72. G. Gauglitz, J. Ingenhoff, Design of new integrated optical substrates for immuno-analytical applications. Fresenius' J. Anal. Chem. **349**, 355–359 (1994)
73. G. Gauglitz, A. Brecht, G. Kraus, W. Nahm, Chemical and biochemical sensors based on interferometry at thin (multi-) layers. Sensor. Actuat. B **11**, 21–27 (1993)
74. C. Pacholski, M. Sartor, M.J. Sailor, F. Cunin, G.M. Miskelly, Biosensing using porous silicon double-layer interferometers: reflective interferometric Fourier transform spectroscopy. J. Am. Chem. Soc. **127**, 11636–11645 (2005)
75. C. Pacholski, C. Yu, G.M. Miskelly, D. Godin, M.J. Sailor, Reflective interferometric Fourier transform spectroscopy: a self-compensating label-free immunosensor using double-layers of porous SiO_2. J. Am. Chem. Soc. **128**, 4250–4252 (2006)
76. F. Cunin, T.A. Schmedake, J.R. Link, Y.Y. Li, J. Koh, S.N. Bhatia, M.J. Sailor, Biomolecular screening with encoded porous silicon photonic crystals. Nat. Mater. **1**, 39–41 (2002)
77. A. Jane, R. Dronov, A. Hodges, N.H. Voelcker, Porous silicon biosensors on the advance. Trends Biotechnol. **27**, 230–239 (2009)
78. T. Kumeria, D. Losic, Controlling interferometric properties of nanoporous anodic aluminium oxide. Nanoscale Res. Lett. **7**, 88 (2012)
79. S.D. Alvarez, C.P. Li, C.E. Chiang, I.K. Schuller, M.J. Sailor, A label-free porous alumina interferometric immunosensor. ACS Nano **3**, 3301–3307 (2009)

80. F. Casanova, C.E. Chiang, C.P. Li, I.V. Roshchin, A.M. Ruminski, M.J. Sailor, Gas adsorption and capillary condensation in nanoporous alumina films. Nanotechnology **19**, 315709 (2008)
81. S. Pan, L.J. Rothberg, Interferometric sensing of biomolecular binding using nanoporous aluminum oxide templates. Nano Lett. **3**, 811–814 (2003)
82. T. Kumeria, M.D. Kurkuri, K.R. Diener, L. Parkinson, D. Losic, Label-free reflectometric interference microchip biosensor based on nanoporous alumina for detection of circulating tumour cells. Biosens. Bioelectron. **35**, 167–173 (2012)
83. T. Kumeria, D. Losic, Reflective interferometric gas sensing using nanoporous anodic aluminium oxide (AAO). Phys. Status Solidi RRL **5**, 10–11 (2011)
84. R. Dronov, A. Jane, J.G. Shapter, A. Hodges, N.H. Voelcker, Nanoporous alumina-based interferometric transducers ennobled. Nanoscale **3**, 3109–3114 (2011)
85. A. Santos, T. Kumeria, D. Losic, Optically optimized photoluminescent and interferometric biosensors base on nanoporous anodic alumina: a comparison. Anal. Chem. **85**, 7904–7911 (2013)
86. T. Kumeria, A. Santos, D. Losic, Ultrasensitive nanoporous interferometric sensor for label-free detection of gold(III) ions. ACS Appl. Mater. Interfaces **5**, 11783–11790 (2013)
87. G. Macias, L.P. Hernández-Eguía, J. Ferré-Borrull, J. Pallares, L.F. Marsal, Gold-coated ordered nanoporous anodic alumina bilayers for future label-free interferometric biosensors. ACS Appl. Mater. Interfaces **5**, 8093–8098 (2013)
88. T. Kumeria, M.M. Rahman, A. Santos, J. Ferré-Borrull, L.F. Marsal, D. Losic, Structural and optical nanoengineering of nanoporous anodic alumina rugate filters for real-time and label-free biosensing applications. Anal. Chem. **86**, 1837–1844 (2014)
89. T. Kumeria, M.M. Rahman, A. Santos, J. Ferré-Borrull, L.F. Marsal, D. Losic, Nanoporous anodic alumina rugate filters for sensing of ionic mercury: toward environmental point-of-analysis systems. ACS Appl. Mater. Interfaces **6**, 12971–12978 (2014)
90. T. Kumeria, K. Gulati, A. Santos, D. Losic, Real-time and *in situ* drug release monitoring from nanoporous implants under dynamic flow conditions by reflectometric interference spectroscopy. ACS Appl. Mater. Interfaces **5**, 5436–5442 (2013)
91. A. Santos, M. Alba, M.M. Rahman, P. Formentín, J. Ferré-Borrull, J. Pallarès, L.F. Marsal, Structural tuning of photoluminescence in nanoporous anodic alumina by hard anodization in oxalic and malonic acids. Nanoscale Res. Lett. **7**, 228 (2012)
92. Y.B. Li, M.J. Zheng, L. Ma, High-speed growth and photoluminescence of porous anodic alumina with controllable interpore distances over a large range. Appl. Phys. Lett. **91**, 073109 (2007)
93. Y. Du, W.L. Cai, C.M. Mo, J. Chen, L.D. Zhang, X.G. Zhu, Preparation and photoluminescence of alumina membranes with ordered pore arrays. Appl. Phys. Lett. **74**, 2951–2953 (1999)
94. G.S. Huang, X.L. Wu, Y.F. Mei, X.F. Shao, G.C. Siu, Strong blue emission from anodic alumina membranes with ordered nanopore array. J. Appl. Phys. **93**, 582–585 (2003)
95. N.I. Mukhurov, S.P. Zhvavyi, S.N. Terekhov, A.Y. Panarin, I.F. Kotova, P.P. Pershukevich, I.A. Khodasevich, I.V. Gasenkova, V.A. Orlovich, Influence of electrolyte composition on photoluminescent properties of anodic aluminum oxide. J. Appl. Spectrosc. **75**, 214–218 (2008)
96. Z. Li, K. Huang, Optical properties of alumina membranes prepared by anodic oxidation process. J. Lumin. **127**, 435–440 (2007)
97. R.P. Jia, Y. Shen, H.Q. Luo, X.G. Chen, Z.D. Hu, D.S. Xue, Enhanced photoluminescence properties of morin and trypsin absorbed on porous alumina films with ordered pore array. Solid State Commun. **130**, 367–372 (2004)
98. C.L. Feng, X. Zhong, M. Steinhart, A.M. Caminade, J.P. Majoral, W. Knoll, Graded-bandgap quantum-dot-modified nanotubes: a sensitive biosensor for enhanced detection of DNA hybridization. Adv. Mater. **19**, 1933–1936 (2007)

99. A. Santos, V.S. Balderrama, M. Alba, P. Formentín, J. Ferré-Borrull, J. Pallarès, L.F. Marsal, Nanoporous anodic alumina barcodes: toward smart optical biosensors. Adv. Mater. **24**, 1050–1054 (2012)
100. A. Santos, G. Macías, J. Ferré-Borrull, J. Pallarès, L.F. Marsal, Photoluminescent enzymatic sensor based on nanoporous anodic alumina. ACS Appl. Mater. Interfaces **4**, 3584–3588 (2012)